2022

Lateral-Torsional Instability and Biaxial Bending of Imperfect FRP I-Beams

Jodi Knorowski

Stella B. Bondi

Zia Razzaq
Old Dominion University, zrazzaq@odu.edu

Original Publication Citation

Knorowski, J., Bondi, S. B., & Razzaq, Z. (2022). Lateral-torsional instability and biaxial bending of imperfect FRP I-beams. *European Journal of Engineering and Technology Research*, *7*(6), 29-34. https://doi.org/10.24018/ejeng.2022.7.6.2687

Lateral-Torsional Instability and Biaxial Bending of Imperfect FRP I-Beams

Jodi Knorowski, Stella B. Bondi, and Zia Razzaq

***Abstract* — This paper presents the outcome of a theoretical and experimental study of the behavior of Fiber Reinforced Polymer (FRP) I-beams exposed to lateral-torsional instability or when subjected to biaxial bending. Laboratory experiments involved the application of vertical and horizontal static loads to a 4 x 4 x ¼ in. I-beam with various lengths and the resulting deflections were recorded. Governing biaxial flexure and torsion differential equations were modified to account for the presence of initial imperfections and subsequently solved using a central finite-difference scheme. The theoretical predictions of the beam behavior were found to be in good agreement with what was observed in the laboratory.**

***Keywords* —Biaxial, Fiber Reinforced Polymer, I-beam, Imperfect, Lateral-Torsional Instability.**

I. Introduction

A number of research studies are available on the flexural-torsional response of fiber-reinforced polymer structural members subjected to bending loads; however, little is available on the behavior of such members under biaxial bending. The biaxial bending itself can induce significant torsional deformations which are not accounted for in the current analytical and design methodologies. Several studies have examined torsional buckling resulting from uniaxial loads applied about the major axis of FRP composite beams [9]. Razzaq et al. have conducted multiple studies on various FRP cross-sections and load conditions using a testing apparatus similar to that used in the current research. One study investigated a channel section that was subjected to a pair of vertical loads applied symmetrically about the mid-span of the beam [7]. In another study, Razzaq et al. [9] applied a single vertical load at the mid-span of an FRP I-beam of different lengths. The experimental data were verified with a maximum moment equation derived from the American Institute of Steel Construction (AISC) Manual.

Qiao [5] applied a point load through the shear center at the free end of a cantilevered FRP beam to determine the torsional buckling load capacity of the member. Various beam spans and geometries were experimentally tested in order to verify derived theoretical equations based on non-linear plate theory. Ragheb [6] in an effort to improve the local buckling capacity of an FRP I- beam, added flange lips to the compression flange. The failure mode for the member was buckling, so finding a way to increase the buckling load would increase the load capacity of the beam. Using a finite element analysis, Ragheb found the addition of flange lips successfully increased the buckling load of the beam.

Sapkás [8] investigated lateral-torsional buckling of a composite I-beam under various load conditions and boundary conditions. A simply supported beam was analyzed with applied end moments, a uniformly distributed load, a single point load at the midpoint, and a pair of point loads applied symmetrically about the midpoint. A cantilever beam was analyzed with a uniformly distributed load and a point load at the free end. A finite element analysis and references to previous experimental data were used to verify the derived buckling load equations. Sapkás also found that the effect of shear deformations could significantly reduce the lateral-torsional buckling load.

Nordin [4] applied a pair of point loads symmetrically about the midpoint of a hybrid glass-FRP I-beam and examined the resulting mid-span deflections. To fabricate this beam, the glass-FRP I-beam was retrofitted with carbon fiber on the tensile flange and concrete on the compressive flange. A theoretical analysis was conducted based on the linear behavior of a concrete beam. The transform area method was used to convert the material properties of FRP and carbon to concrete. This analysis was verified with experimental results. During the experiment, the beam was unstable in the lateral direction and had to be reinforced with braces. Nordin concluded that this hybrid could be a cost-effective alternative to steel and concrete hybrid beams, as long as careful attention was paid to lateral instability.

Ellingwood [2] discussed the uncertainty of FRP composites which makes it difficult to create a design code for the material. He developed a probability-based approach to FRP composite design in which load and resistance factors were modeled as random variables. He concluded that it was feasible to develop probability-based limit state design criteria for FRP structures; however, extensive research and testing would be needed to achieve this goal.

In order to theoretically predict the load-deflection response of a biaxially loaded FRP I-section beam, three simultaneous governing differential equations are needed. The first two are flexural equilibrium equations that include induced torsional effects. The third equation enforces torsional equilibrium including higher-order torsional effects. An exact solution for the three coupled differential equations does not exist in the literature. In the present study, numerical results based on a numerical approach are presented including the effects of initial geometric imperfections in the beam.

Submitted on December 01, 2021.
Published on November 10, 2022.
J. Knorowski, WPD Consulting Engineers & Associates, USA.
(corresponding e-mail: jodi.knorowski@gmail.com)
S. B. Bondi, Naval Sea Systems Command, USA.
(e-mail: stella.bondi@yahoo.com)
Z. Razzaq, Old Dominion University, USA.
(e-mail: zrazzaq@odu.edu).

II. Experimental Procedure

The FRP beam studied was 4 x 4 x 0.25 in. I-beam manufactured by Creative Pultrusions, Inc. in Alum Bank, PA. The section and material properties are given in Table I.

The I-beam was simply supported to prevent lateral and vertical displacements at the supports as shown in Fig. 1.

Dial gages were used to record mid-span deflections that were then used to calculate the vertical and lateral deflections, as well as the angle of twist at the mid-span of the I-beam. Major-axis bending of the member was achieved by applying a pair of point loads, P, symmetrically about the mid-span of the beam (Fig 1) using hydraulic means. Fig. 2 shows the test setup.

A hydraulic pump was connected to a pair of hydraulic jacks that were in turn bolted to the top of a fixed-end steel beam. The connections between the hydraulic pump and the two hydraulic jacks allowed equal pressure to develop in each hydraulic jack when the system was activated with the hydraulic pump. The pistons of the hydraulic jacks were oriented upward. Steel plates were fixed to the top of the pistons and transferred loads from the hydraulic jacks to steel tie rods. Load cells were mounted between the hydraulic jacks and the steel plates. Fig. 3 shows the lower ends of the steel tie rods that are connected to another steel plate.

One-inch diameter steel rods were welded to the middle of these steel plates. Two aluminum loading plates were fabricated to encase the I-Beam at the points of loading. The welded steel rods made contact with the aluminum loading plates directly under the shear center of the I-Beam, creating a point load. The FRP I-beam was then loaded incrementally. Deflections were recorded for each load level. Unsupported beam lengths of 64, 82, and 100 inches were tested.

To apply a biaxial load, a lateral load, H, is applied at the mid-span of the I-beam in combination with the vertical loads, P (Fig. 1). The lateral load is applied using a pulley system. A schematic of this system is shown in Fig. 4.

TABLE I: FRP I-Beam Material and Section Properties

Depth (in.)	4.00
Width (in.)	4.00
Flange Thickness (in.)	0.25
Web Thickness (in.)	0.25
Major Axis Moment of Inertia, I_x (in^4)	8.05
Minor Axis Moment of Inertia, I_y (in^4)	2.63
Major Axis Modulus of Elasticity, E_x (psi)	4.35×10^6
Minor Axis Modulus of Elasticity, E_y (psi)	3.10×10^6
Shear Modulus, G (psi)	4.03×10^5

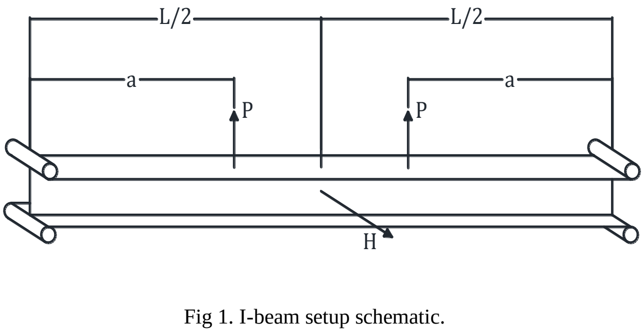

Fig 1. I-beam setup schematic.

Fig 2. Test Setup.

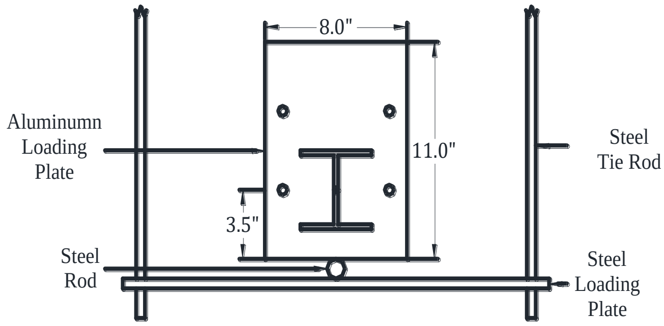

Fig 3. Point Load Attachment.

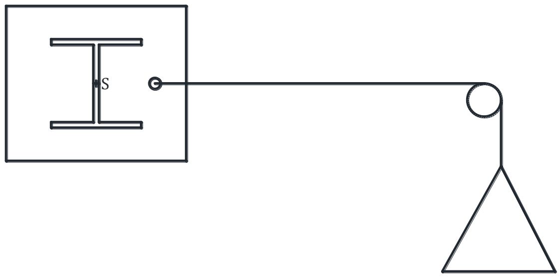

Fig 4. Schematic of Lateral Load.

The pulley was anchored to a steel rod that allowed for height adjustments. A steel cable ran through the pulley and attached to a fabricated steel container. The opposite end of the steel cable was connected to an aluminum loading plate that encased the I-beam at its midpoint. The cable connected to the aluminum loading plate at the shear center of the I-beam cross section. The height of the steel rod was adjusted so that the cable was level. Weight equaling 300 lbs. was added to the steel container and held constant. The hydraulic pump was used to increase the loads about the major axis of the I-beam. At each load increment, the corresponding deflection and strain readings were recorded. Unsupported beam lengths of 64 inches, 82 inches, and 100 inches were tested.

III. EXPERIMENTAL RESULTS

Table II, Table III, and Table IV present the vertical deflection, V, lateral deflection, U, and angle of twist, φ, which result from processing the deflection values recorded experimentally when only the vertical loads were applied. Fig. 5, Fig. 6, and Fig. 7 illustrate the relationship between the vertical load and deflection for the I-beam of various lengths, loaded only about the major axis. Table V, Table VI, and Table VII present the vertical deflection, lateral deflection, and angle of twist, resulting from processing the deflection values recorded experimentally when biaxial loads were applied.

TABLE II: VERTICAL LOAD (L = 64 INCHES)

Vertical Load, P		Midspan Deflections		
Voltage (mV)	Load (lbs)	V (in.)	U (in.)	φ (Rads.)
0	0	0	0	0
30.9	119.7	0.0303	0.0014	0.0017
62.6	242.8	0.0640	0.0030	0.0048
90.1	349.2	0.0917	0.0046	0.0069
122.0	472.8	0.1260	0.0076	0.0098
150.3	582.8	0.1547	0.0113	0.0125
181.1	702.2	0.1883	0.0155	0.0149
212.0	821.9	0.2206	0.0201	0.0187
240.0	930.4	0.2486	0.0252	0.0221
270.3	1048.0	0.2805	0.0307	0.0260
300.7	1165.6	0.3141	0.0387	0.0306
329.0	1275.4	0.3443	0.0457	0.0356
361.7	1402.1	0.3791	0.0563	0.0444
390.0	1511.9	0.4099	0.0674	0.0518
420.3	1629.5	0.4424	0.0842	0.0637
449.3	1741.9	0.4741	0.1080	0.0798
478.3	1854.4	0.5039	0.1488	0.1152
507.3	1966.8	0.5603	0.1837	0.1346

TABLE III: VERTICAL LOAD (L = 82 INCHES)

Vertical Load, P		Midspan Deflections		
Voltage (mV)	Load (lbs)	V (in.)	U (in.)	φ (Rads.)
0	0	0	0	0
30.7	118.9	0.0700	0.0061	0.0020
61.0	236.6	0.1400	0.0139	0.0042
90.8	352.1	0.2055	0.0245	0.0071
119.8	464.6	0.2744	0.0353	0.0107
150.8	584.7	0.3419	0.0476	0.0145
180.8	701.0	0.4091	0.0639	0.0201
209.3	811.5	0.4719	0.0881	0.0298
240.7	933.0	0.5386	0.1416	0.0533
254.0	984.7	0.6128	0.1905	0.0521
263.5	1021.5	0.6321	0.2267	0.0755

TABLE IV: VERTICAL LOAD (L = 100 INCHES)

Vertical Load, P		Midspan Deflections		
Voltage (mV)	Load (lbs)	V (in.)	U (in.)	φ (Rads.)
0	0	0	0	0
31.4	121.6	0.1190	0.0070	0.0058
59.9	232.1	0.2336	0.0200	0.0116
91.3	353.9	0.3582	0.0432	0.0190
120.7	467.8	0.4801	0.0850	0.0269
148.5	575.6	0.5634	0.1690	0.1219
150.8	584.6	0.5672	0.1504	0.1354

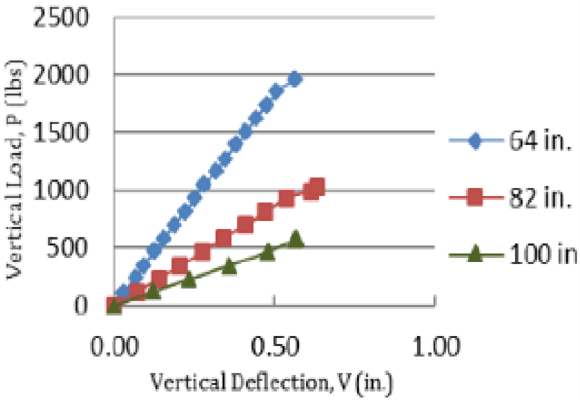

Fig. 5. Vertical Load versus Vertical Deflection.

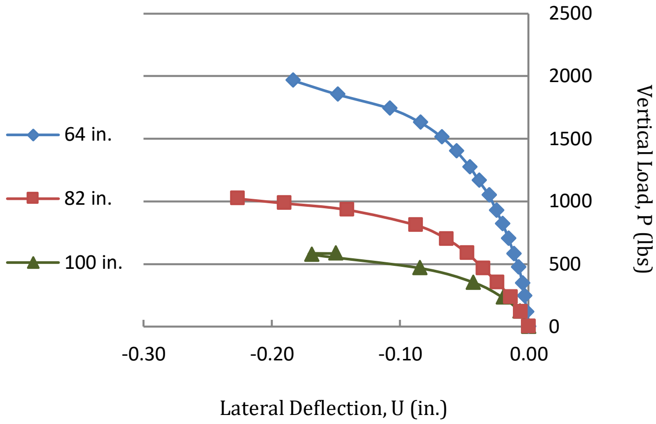

Fig. 6. Vertical Load versus Lateral Deflection.

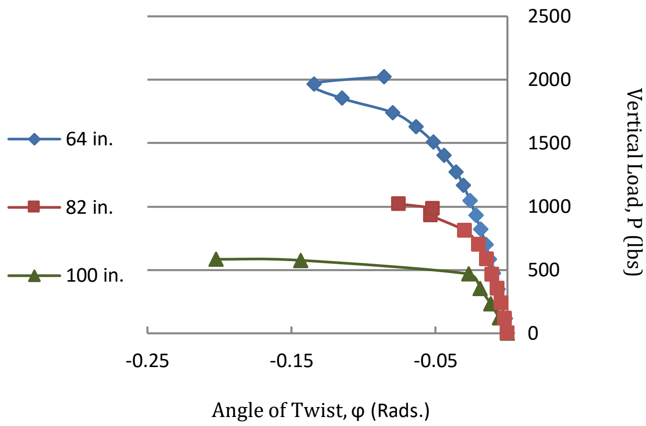

Fig 7. Vertical Load versus Angle of Twist.

TABLE V: BIAXIAL LOADING (L = 64 INCHES)

Lateral Load, H, constant at 300 lbs				
Vertical Load, P		Midspan Deflections		
Voltage (mV)	Load (lbs)	V (in.)	U (in.)	φ (Rads.)
0	0	0.0122	-0.2281	-0.0097
30.8	119.3	0.0438	-0.2318	-0.0099
61.9	239.8	0.0722	-0.2361	-0.0111
91.0	352.7	0.1076	-0.2401	-0.0103
121.1	469.5	0.1388	-0.2442	-0.0107
151.5	587.4	0.1669	-0.2483	-0.0118
180.5	699.9	0.2016	-0.2503	-0.0116
210.3	815.4	0.2344	-0.2528	-0.0121
241.3	935.6	0.2663	-0.2557	-0.0127
270.0	1046.7	0.2977	-0.2586	-0.0133
300.3	1164.3	0.3305	-0.2624	-0.0142
332.3	1288.4	0.3666	-0.2662	-0.0151
360.0	1395.6	0.3959	-0.2697	-0.0160
390.0	1511.9	0.4295	-0.2735	-0.0174
420.0	1628.2	0.4647	-0.2760	-0.0194

TABLE VI: BIAXIAL LOADING (L = 82 INCHES)

Lateral Load, H, constant at 300 lbs				
Vertical Load, P		Midspan Deflections		
Voltage (mV)	Load (lbs)	V (in.)	U (in.)	φ (Rads.)
0	0	0.0078	-0.4744	-0.0065
31.2	121.0	0.0697	-0.4801	-0.0112
60.5	234.7	0.1307	-0.4903	-0.0146
91.4	354.2	0.1929	-0.5020	-0.0190
120.7	468.0	0.2493	-0.5130	-0.0241
150.7	584.2	0.3046	-0.5274	-0.0308
181.0	701.8	0.3697	-0.5435	-0.0372
211.0	818.0	0.4045	-0.5667	-0.0539
242.7	940.7	0.4817	-0.5993	-0.0684
272.3	1055.8	0.6439	-0.6696	-0.0864
290.7	1126.8	0.8810	-0.7507	-0.1199

TABLE VII: BIAXIAL LOADING (L = 100 INCHES)

Lateral Load, H, constant at 300 lbs				
Vertical Load, P		Midspan Deflections		
Voltage (mV)	Load (lbs)	V (in.)	U (in.)	φ (Rads.)
0	0	0.0432	-0.6291	-0.0018
30.9	119.7	0.1222	-0.6395	-0.0125
60.6	234.8	0.2433	-0.6558	-0.0183
90.6	351.1	0.2827	-0.6717	-0.0294
120.8	468.2	0.3474	-0.6939	-0.0417
150.8	584.7	0.4175	-0.7197	-0.0570
180.8	700.8	0.5006	-0.7537	-0.0764
210.0	814.1	0.5047	-0.7987	-0.1192
230.5	893.6	0.5564	-0.8571	-0.1645
240.0	930.4	0.8374	-0.9532	-0.2088

Fig. 8, Fig. 9 and Fig. 10 depict the relationship between the vertical load versus deflection for the I-beam of various lengths, loaded biaxially.

IV. THEORETICAL STUDY

The experimental behavior of the beams was verified theoretically using governing differential equations and the central finite-difference method to generate vertical deflections, lateral deflections, and the angle of twist at the mid-span of the beam. The governing differential equations for elastic analysis of a biaxially loaded member when applied at any point, i, along the length of a member [7] take the form of (1), (2) and (3).

$$E_x\, I_x \frac{d^2 V_i}{dz_i^{\,2}} + \varphi_i M_{yi} = -M_{xi} \qquad (1)$$

$$E_y\, I_y \frac{d^2 U_i}{dz_i^{\,2}} + \varphi_i M_{xi} = M_{yi} \qquad (2)$$

$$E_y I_\omega \frac{d^3 \varphi_i}{dz_i^{\,3}} - (GK_T + K)\frac{d\varphi_i}{dz_i} + M_{xi}\frac{dU_i}{dz_i} + M_{yi}\frac{dV_i}{dz_i} = -M_{zi} \qquad (3)$$

where E_x, E_y, I_x, I_y, and G are given in Table I. The St. Venant's Torsion constant, KT, and the Warping Moment of Inertia, Iω, can be found using equations found in Reference [7]. The Wagner effect term, K, equals zero due to the symmetry of an I-beam cross-section. The vertical deflection, V, the lateral deflection, U, and the angle of twist, φ, vary along the length of the beam and with different load increments. The M_{xi} term is the major axis bending moment at a specific point, i, along the member due to the vertical load, P. The M_{yi} term is the minor-axis bending moment at a specific point, i, along the member due to the lateral load, H.

The M_{zi} term is the moment at a specific point, i, along the member length due to applied torque.

Sirjani [10] gave consideration to the reference load height, y_0*, as it applied to these governing equations. (4) shows the modification to (3) based on his conclusions:

$$E_y I_w \frac{d^3 \varphi_i}{dz_i^{\,3}} - (GK_T + K)\frac{d\varphi_i}{dz_i} + M_{xi}\frac{dU_i}{dz_i} + M_{yi}\frac{dV_i}{dz_i} + P\left[U_{L/2} - y_0{}^{*}\varphi_{L/2} - U_i\right] = -M_{zi} \qquad (4)$$

where $U_{L/2}$ and $\varphi_{L/2}$ are the lateral deflection and angle of twist at the mid-span of the beam, respectively. When an in-plane load is applied to a 'perfect' member, the member will react only in that plane. Experimentation showed that under in-plane loading, out-of-plane displacement and twisting occurred due to possible material irregularities and initial imperfections in the experimental test setup. Fig. 11 is a schematic illustration of an 'imperfect' I-beam cross-section that includes initial imperfections in comparison to a 'perfect' I-beam cross-section.

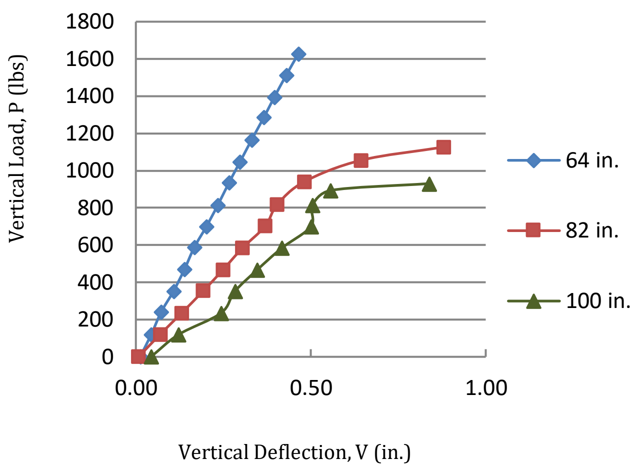

Fig. 8. Vertical Load versus Vertical Deflection.

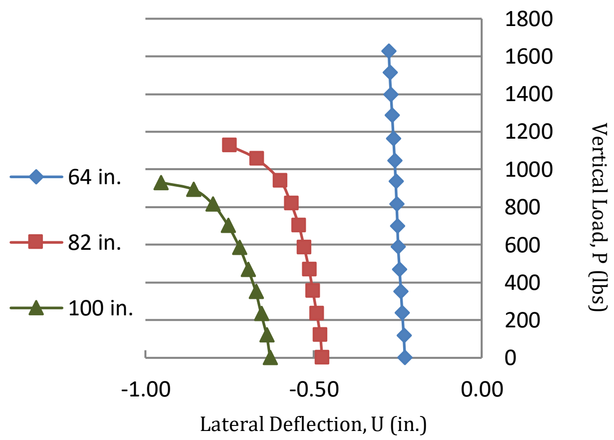

Fig. 9. Vertical Load versus Lateral Deflection.

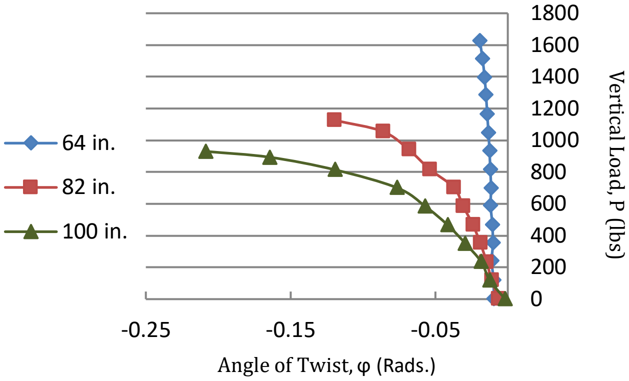

Fig. 10. Vertical Load versus Angle of Twist.

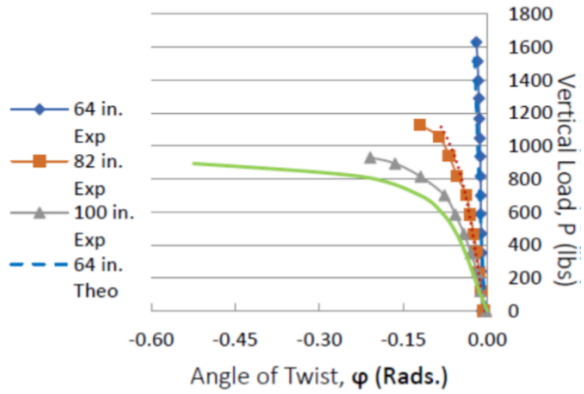

Fig. 12. Experimental and Theoretical Relations between Vertical Load and Angle of Twist for Biaxially Loaded Beams.

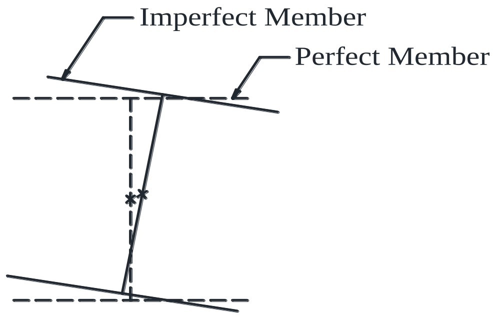

Fig. 11. Imperfect versus Perfect Member.

To incorporate these effects in the theoretical analysis, initial imperfection factors were added to (4) which then become (5) and (6), respectively, over the domains [0, a] and [a, L/2].

$$E_y I_w \frac{d^3\varphi_i}{dz_i^3} - GK_T \frac{d\varphi_i}{dz_i} + M_{xi}\frac{dU_i}{dz_i} + M_{yi}\frac{dV_i}{dz_i} + P\left[U_{L/2} - y_0{}^*\varphi_{L/2} - U_i\right] + P(y_0{}^*)\varphi_i + HV_i = Hv_{0i}\sin\left(\frac{\pi z_i}{L}\right) - P(y_0{}^*)\varphi_{0i}\sin\left(\frac{\pi z_i}{L}\right) \quad (5)$$

$$E_y I_w \frac{d^3\varphi_i}{dz_i^3} - GK_T \frac{d\varphi_i}{dz_i} + M_{xi}\frac{dU_i}{dz_i} + M_{yi}\frac{dV_i}{dz_i} + P\left[U_{L/2} - y_0{}^*\varphi_{L/2} - U_i\right] + HV_i = Hv_{0i}\sin\left(\frac{\pi z_i}{L}\right) \quad (6)$$

where v_{0i} and φ_{0i} are initial vertical and rotation imperfections at the mid-span of the beam. The following boundary and symmetry conditions are applied to Equations 1, 2, 5, and 6 and then solved simultaneously using the central finite-difference method:

$$V_0 = U_0 = \varphi_0 = 0 \quad (7)$$

$$V_0{}'' = U_0{}'' = \varphi_0{}'' = 0 \quad (8)$$

$$V_N{}' = U_0{}' = \varphi_0{}' = 0 \quad (9)$$

Fig. 12 illustrates a comparison of the experimental and theoretically predicted vertical load versus the angle of twist relations for biaxially loaded beams of length 64 in., 82 in., and 100 in., respectively.

V. Conclusion

The initial imperfections of a member can have significant effects on the out-of-plane displacements and rotation a member experiences even if only in-plane loads are applied. With the incorporation of factors due to beam imperfections, the solutions based on the governing differential equations are in good agreement with those found experimentally. The finite-difference method provided an effective method for solving the differential equations simultaneously.

Conflict of Interest

Authors declare that they do not have any conflict of interest.

References

[1] American Society of Civil Engineers, *Proposed Design Specification for FRP Structures*, 2012.
[2] Ellingwood BR. Toward Load and Resistance Factor Design for Fiber-Reinforced Polymer Composite Structures. *Journal of Structural Engineering*, 2003: 449-458.
[3] Galambos TV. *Structural Members and Frames*, Englewood Cliffs, NJ: Prentice-Hall, Inc., 1968.
[4] Nordin H, Taljsten B. Testing of Hybrid FRP Composite Beams in Bending. *Composites Part B*, 2004; 35: 27-33.
[5] Qiao P, Zou G, Davalos JF. Flexural-torsional Buckling of Fiber-Reinforced Plastic Composite Cantilever I-beams. *Composite Structures*, 2003; 60: 205-217.
[6] Ragheb W. Improving Local Buckling Capacity of Pultruded I-Beams using Flange Lips. *Journal of Reinforced Plastics and Composites*. 2007; 26(15): 1513-1521.
[7] Razzaq Z, Prabhakaran R, Sirjani MB. Load and Resistance Factor Design (LRFD) Approach for Reinforced-Plastic Channel Beam Buckling. *Composites: Part B*, 1996; 27B (3-4): 361-369.
[8] Sapkás A, Kollár LP. Lateral-torsional Buckling of Composite Beams. *International Journal of Solids and Structures*, 2002; 39: 2939-2963.
[9] Sirjani MB, Razzaq Z. Stability of FRP Beams under Three-point Loading and LRFD Approach. *Journal of Reinforced Plastics and Composites*, 2005; 24(18): 1921-1927.
[10] Sirjani, MB. Fiber Reinforced Plastic Composite Beam Stability and Load and Resistance Factor Design Approach. *PhD Dissertation*, Department of Civil and Environmental Engineering, Old Dominion University, Norfolk, VA 23529, USA, 1998.
[11] *Design Manual of Standard and Custom Fiber Reinforced Polymer Structural Profiles*, (vol 4). Creative Pultrusions Inc., Alum Bank, PA, 2004.

Jodi Knorowski, PE, is a Senior Engineer at WDP Consulting Engineers and Associates, USA. Dr. Stella Bondi is a Research Scientist at NAVSEA in Virginia, USA. Dr. Zia Razzaq, PE, ASCE Fellow, is a Professor of Civil & Environmental Engineering at the Old Dominion University, Virginia, USA.

Dr. Stella Bondi is a Research Scientist at NAVSEA, Dahlgren in Virginia, USA. She received a PhD degree from the Old Dominion University, Norfolk, Virginia, USA in 2007.

Dr. Zia Razzaq is a Professor of Civil and Environmental Engineering at the Old Dominion University, Virginia, USA. He received a DSc degree from Washington University, St. Louis, Missouri, USA in 1974. He is a professional engineer (PE) registered in the Commonwealth of Virginia and was elected Fellow of the American Society of Civil Engineers in 1988.